Microelectronics Failure Analysis
Desk Reference, Sixth Edition
R.J. Ross, editor

Product code: 09110Z

Thermal Failure Analysis by IR Lock-in Thermography

O. Breitenstein
Max Planck Institute of Microstructure Physics, Halle, Germany

C. Schmidt, F. Altmann
Fraunhofer Institute for Mechanics of Materials, Halle, Germany

D. Karg
Thermosensorik GmbH, Erlangen, Germany

Abstract

Thermal infrared (IR) microscopy has experienced a decisive technical improvement by the application of Lock-in Thermography (LIT), which is commercially available for failure analysis by different vendors. Due to its averaging nature, this technique allows the detection of local heat sources at the surface of a few µW corresponding to a local temperature modulation of a few µK. Thus it outperforms other thermal imaging methods, like liquid crystal imaging, fluorescent microthermal imaging, Raman IR-thermography, and steady-state IR thermography, by 2 to 3 orders of magnitude. Thereby, LIT allows to extend the application field of thermal imaging for failure analysis drastically. The emissivity contrast, which obscures the thermal contrast in conventional IR thermography, can be avoided in LIT by displaying the phase image or the 0°/-90° image in a 2-phase measurement. Due to its dynamic nature, lateral heat diffusion (blurring) is considerably reduced in LIT compared to steady-state techniques, depending on the chosen lock-in frequency. The usefulness of Lock-in Thermography is given mainly by the fact that it allows a though relatively coarse (3-5 µm) but very sensitive localization of any leakage current or other local heat source in an IC with a very high success rate without any preparation expense. LIT is also applicable for backside inspection and for detecting sub-surface heat sources. Its spatial resolution can be improved down to 1 µm by applying a solid immersion lens. By using LIT some faults can be localized which are not visible in OBIRCH or light emission microscopy. In this contribution the technique of microscopic IR Lock-in Thermography is described, the basic principles of the interpretation of the results are reviewed, and some typical results illustrating the application of this technique are introduced.

Lock-in Thermography - technique

Lock-in Thermography was invented in 1984 [1] and has been used extensively in non-destructive testing for "looking below the surface" of solid objects [2]. Meanwhile it represents also a standard technique for investigating shunting phenomena in solar cell research and for failure analysis in ICs [3, 4]. Lock-in Thermography means that the power dissipated in the object under investigation is periodically amplitude-modulated, the resulting surface temperature modulation is imaged by a thermo camera running with a certain frame rate f_{fr}, and that the generated IR images are digitally processed according to the lock-in principle. Thus, the effect of LIT is the same as if each pixel of the IR image would be connected with a 2-phase lock-in amplifier. In principle, Lock-in Thermography can also be applied with 1-phase detection, but then some very useful display options like phase imaging are not available. The two primary results of 2-

phase LIT are the image of the in-phase signal $S^{0°}(x,y)$ and that of the out-of-phase (or quadrature) signal $S^{-90°}(x,y)$. In LIT the -90° signal is used instead of the +90° one, since the latter is essentially negative [3]. From these two signals the image of the phase-independent amplitude $A(x,y)$ and the phase image $\Phi(x,y)$ of the surface temperature modulation can easily be derived:

$$A(x,y) = \sqrt{S^{0°}(x,y)^2 + S^{-90°}(x,y)^2} \qquad (1)$$

$$\Phi(x,y) = \arctan\left(\frac{-S^{-90°}(x,y)}{S^{0°}(x,y)}\right) \qquad (2)$$

Note that for Φ the quadrant-correct arctan function has to be used, hence if $S^{0°}(x,y)$ is negative, 180° have to be subtracted from the pure arctan value. Both the 0° and the -90° images are proportional to the magnitude of the temperature modulation, multiplied by the IR-emissivity ε. Therefore in the amplitude image the contrast of a heat source is proportional to its dissipated power, multiplied by ε. The phase image, on the other hand, relies on the quotient of the 0° and the -90° image, hence for isolated heat sources it is independent of the power of the heat source and also of ε. Thus the phase signal is inherently emissivity-corrected. In fact, the phase image is a measure of the time delay of the surface temperature modulation referred to the power modulation, which is indeed independent of the magnitude of the heat source, as long as we have no superposition of the temperature fields of neighbouring heat sources. For the application of LIT in thermal failure analysis this property implies a kind of "dynamic compression" for the phase signal, so that local heat sources with different powers are displayed with a similar signal height. It will be shown below that these properties greatly simplify the interpretation of the results. Note, however, that in metallised regions having a low value of ε also the signal-to-noise ratio of both primary images decreases, hence metallised regions may appear more noisy in the phase image than non-metallised ones. This can be avoided by blackening the surface, which can be done e.g. by colloidal bismuth which is relatively easy to deposit and can easily be removed in an ultrasonic bath [5, 6]. Instead of IR thermography also fluorescent microthermal imaging (FMI) or Moiré thermal imaging can be applied in lock-in mode [7, 8]. These techniques are sometimes called "stabilized" instead of lock-in [8] to make clear that in these dynamic techniques the result can be obtained already after a few lock-in periods or even after one period and not after reaching thermal equilibrium. Note that FMI may provide sub-micron spatial resolution, but it does not allow backside inspection with good spatial resolution, it needs a foreign layer at the surface, and it is about a factor of 10 less sensitive than IR LIT [7]. Stabilized Moiré thermal imaging [8] is a pure backside inspection technique. Its spatial resolution is only in the order of the bulk thickness, and its sensitivity is also well below that of IR LIT.

As an alternative to the phase image in 2-phase LIT, also the 0°/-90° signal ratio may be displayed [5]. Since in microscopic regions the -90° signal has a very poor spatial resolution, this image can be taken as a local measure of the IR emissivity ε. Therefore the 0°/-90° image is also inherently emissivity-corrected, just as the phase image. In contrast to the latter, however, the 0°/-90° image shows a better spatial resolution, the signal height reflects the power of local heat sources, and it even can be used directly for correcting the thermal blurring by applying image deconvolution techniques [5].

Fig. 1 shows how the image data are evaluated in LIT to obtain the primary signals $S^{0°}$ (or $S^{-90°}$) for each pixel. In simplest case the supply voltage V_{CC} of the device is switched periodically on and off to a well-defined value for realizing the periodic heat modulation. If

V_{CC} is not allowed to be switched completely off, it also can be square-wave modulated between two values. Sine-modulation of V_{CC} would be also possible, but it gives no advantage to square-modulation and is even not useful, since then the device is not investigated at a well-defined supply voltage. At least 4 frames per lock-in period have to be evaluated, since according to the Shannon sampling theorem at least two samples per period are necessary, which holds for each phase position (0° and -90°). The actual 2-phase lock-in correlation consists of multiplying the information of each incoming image by weighting factors in two logical channels and summing up these products in two separate frame storages. In one channel the weighting factors are approximating a sine- and in the other one a (-cosine)-function [3] (harmonic correlation). Other correlation functions (e.g. square-shaped) are also feasible, but for them the splitting into an amplitude and a phase image according to (1) and (2) is not correct anymore. Fig. 1 (a) illustrates the general case of harmonic correlation for the in-phase signal for the case of 12 frames per lock-in period. Here the line symbolizes the basic harmonic of the in-phase part of the local temperature modulation, which is detected by this procedure, and the squares symbolize the sampling moments and the magnitudes of the weighting factors. Here, in the first half-period the weighting factors are positive and in the second half-period they are negative. After each period (dashed line) the procedure repeats. For obtaining the -90° signal a (-cosine)-function has to be used in Fig. 1 (a) for the weighting factors. For obtaining the highest possible detection sensitivity, the IR camera is always running at its highest possible frame rate f_{fr} and the lock-in frequency $f_{lock\text{-}in}$ is adjusted by choosing an appropriate number of frames per period. Since the sum of all weighting factors is zero, this correlation provides a perfect suppression of the steady-state (topography) image, which is basically governed by the emissivity contrast. Nevertheless, the primary LIT images $S^{0°}$ and $S^{-90°}$ still contain the emissivity contrast $\varepsilon(x,y)$ as a factor.

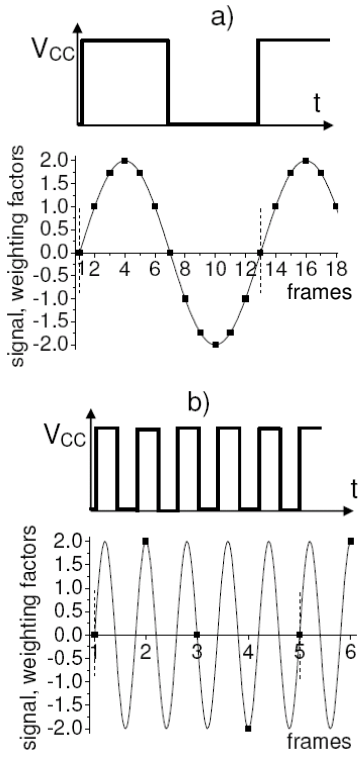

Fig. 1: Scheme of the Lock-in Thermography correlation (0° signal), (a) conventional, (b) undersampling

The limitation of the conventional LIT correlation shown in Fig. 1 (a) is that, since we need at least 4 frames per lock-in period, the maximum possible lock-in frequency is $f_{lock\text{-}in} = f_{fr}/4$, which is 25 Hz for a typical frame rate of 100 Hz. If several local heat sources are lying close to each other, it may be necessary to further increase $f_{lock\text{-}in}$ for further reducing thermal blurring. This limitation can be overcome by applying the "undersampling" timing strategy sketched in Fig. 1 (b). Here only one sample is taken in each lock-in period (or even every few periods), but its phase position varies from period to period. The evaluation occurs as for conventional LIT. By applying this technique lock-in frequencies in

the kHz-range may be realized even for full frame LIT imaging. Note that this reduction of blurring reduces the sensitivity, since the magnitude of the LIT signal always reduces with increasing lock-in frequency [3].

The effective spatial resolution

If Lock-in Thermography is applied for failure analysis of integrated circuits, a decisive limitation is its limited spatial resolution. For a point-like heat source lying at the surface of a device, the surface temperature modulation field at a small lateral distance r from the source reduces with $1/r$, independent of the thermal diffusion length [3]. Hence, even for low lock-in frequencies point-like heat sources at the surface can be localized sharply, only the extension of the halo around depends on the lock-in frequency. Lateral heat spreading is more disturbing for spatially extended heat sources [3]. This heat spreading can be considered even as an advantage since it guarantees that spatially small heat sources cannot be overlooked in a low-magnification survey image. Note, however, that the critical point is not the resolution of the lock-in images, which anyway may appear more or less blurred due to lateral heat spreading or because the actual heat source may lay at a certain depth below the surface. Even in such a case, if a heat source is point-like, the position of its center can usually be estimated up to an accuracy of 1 pixel by finding the center of gravity of the blurred spot. The main problem with spatial resolution is that the operator still needs to be able to navigate on the surface of the IC! Today the layout patterns may be so small that no details can be resolved anymore with a conventional microscope objective in the mid-IR range. Therefore the challenge for improving the spatial resolution is to get a meaningful topography image, which enables an orientation on the surface. Only then local peaks in the lock-in images can be related reliably to the layout of the IC.

The resolution Δx of any optical system is physically limited by diffraction, which is governed by the wavelength λ of the radiation used for imaging. According to the so-called Sparrow Criterion [9], the optical resolution is limited to:

$$\Delta x = \frac{0.5\,\lambda}{n\sin(\theta)} \qquad (3)$$

Here θ is the half-angle of the light-cone to the objective and n is the refractive index of the medium surrounding the sample. The product $n*\sin(\theta)$ is also called "numerical aperture" (NA). For a given magnification factor of the objective, the brightness of an image (hence the signal-to-noise ratio of the measurement) increases with the square of $\sin(\theta)$, since the number of photons reaching the detector increases with an increasing solid angle used by the objective. Even for high brilliance microscope objectives, θ can hardly be larger than 30 to 45° for technical reasons, therefore $\sin(\theta)$ is at best between 0.5 and 0.7. Hence, in air (n = 1) the optical resolution can be only slightly better than the wavelength λ used for imaging. Therefore midwave IR cameras working in the 3-5 µm range show a better spatial resolution than longwave cameras working at 8-12 µm. Unfortunately, for samples being close to room temperature, in the mid range the light intensity exponentially increases with wavelength. So the dominant part of the light is concentrated close to 5 µm and only a negligible part appears at 3 µm. Therefore, for a good microscope objective with NA = 0.7 (+/- 45° light acceptance angle), according to (3) the diffraction-limited spatial resolution limit for λ = 5 µm is Δx = 3.6 µm. This limit can be improved to close to 1 µm by applying a solid immersion lens (SIL) [10, 11]. This is in simplest case a half-bowl made from silicon or germanium which is placed with its plane bottom face on the plane surface of the device.

This lens provides an additional optical magnification at least equal to the diffraction index n of the material, which is about 3.5 for Si and 4 for Ge. Since here the object is "immersed" in the SIL-material, the wavelength of the light is smaller by n there and the NA increases by this factor. Thus, if the slit between the surface and the SIL is well below 1 µm, surface structures with dimensions down to 1 µm can be seen, and for point-like heat sources at the surface the spots in the LIT image are getting correspondingly smaller. SILs can be applied both at the front or at the back surface of devices, if they are accurately flat polished.

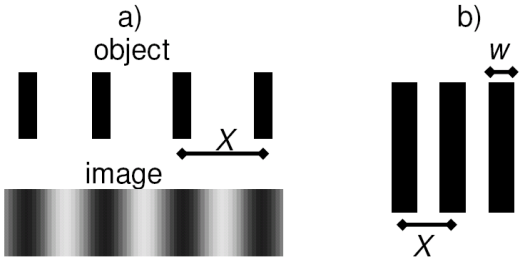

Fig. 2: (a) Line object and its image close to the resolution limit, (b) USAF pattern showing the spatial resolution X and the "line and space distance" *w*

Note that the term "diffraction-limited spatial resolution" refers to the minimum distance of two neighboring small spots or lines (i.e. a "line pair"), which can be separated from each other. If more than two parallel lines are used, the right line of the left line pair coincides with the left line of the right pair, hence e.g. "288 line pairs/mm" actually means 288 lines/mm, corresponding to a line distance (center-to-center) of X = 3.47 µm. If such a periodic arrangement is imaged with an objective close to its resolution limit, the brightness is sine-modulated with a spatial frequency of $f = 1/X$, which is the basic spatial harmonic, see Fig. 2 (a). All higher spatial frequencies are suppressed since we have assumed that these details are below the diffraction-limited spatial resolution. The decisive point is that the spatial frequency f is only dependent on the center-to-center distance of the lines X but not on the line width w or the line distance $X - w$. Only the intensity of the basic spatial harmonic compared to higher harmonics depends on w. It is highest if $w = X/2$ holds, hence if the lines have a distance equal to their width. This is realized e.g. in the elements of the well-known USAF resolution target, one of them sketched in Fig. 2 (b). Here 3 lines with a center-to-center distance X are displayed with a distance of $X/2$ in between. For 288 line pairs/mm this distance is about 1.74 µm. If these lines can be observed separately, the thereby proven spatial resolution is not $X/2$, but it is the center-to-center line distance X! Some authors consider the "line and space distance" $w = X/2$ as a measure of the resolution [11], but this overestimates the spatial resolution by a factor of 2.

Another interesting question is which magnification factor M of the lens must be used for making use of the diffraction-limited spatial resolution. One might think that a lens leading to an object pixel distance of Δx according to (3) should be sufficient ($M > 4.2\times$ for a pitch size of 15 µm and Δx = 3.6 µm), but this is wrong. According to Shannon's sampling theorem at least two samples are necessary per spatial wavelength in order to have at least one pixel at the maximum and one at the minimum of a periodic contrast, see Fig. 2 (a). Thus, for a pitch size of 15 µm and Δx = 3.6 µm the lens must have a magnification of at least $M = 8.4\times$ for reaching the diffraction-limited spatial resolution. An even higher magnification factor may still improve the visual image quality, but for LIT it also degrades the signal-to noise ratio, which reduces with $1/M^2$ [9].

Typical results

Fig. 3 shows the amplitude image of a Hall sensor circuit (a), the corresponding phase image (b), the 0°/-90° image (c, detail), and the

power distribution (d) numerically deconvoluted from (c).

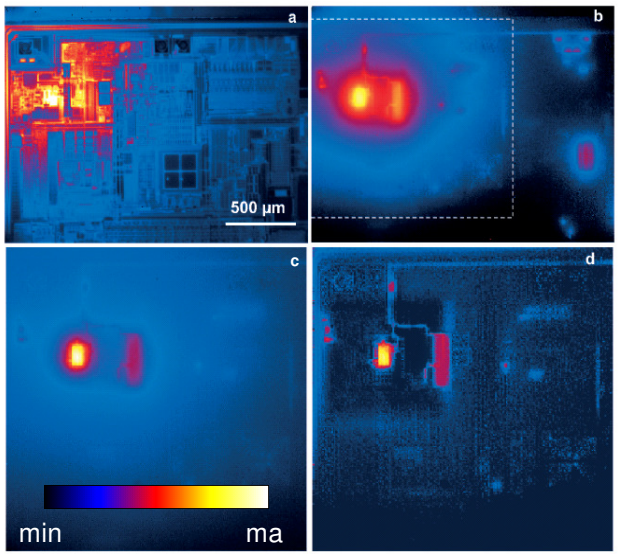

Fig. 3: Amplitude image (a), phase image (b), ε-corrected 0° image (c; 0°/-90° image from the region indicated in b), and power distribution (d), numerically deconvoluted from (c), of a hall sensor circuit; supply voltage pulsed with 22 Hz

All details visible in Fig. 3 are due to the normal operation of this circuit. The selected region displayed in (c) and (d) is indicated in (b). The measurement was performed at a lock-in frequency of 22 Hz within a few minutes. We see that the amplitude image (a) is indeed strongly affected by the emissivity contrast caused by the metallization pattern. Note that due to the lock-in technique the steady-state IR image (topography image) is already perfectly suppressed even in the amplitude image (a). Hence, the bright regions outside of the heat source positions, modulated by the local emissivity contrast, are caused by the inevitable lateral heat conduction-induced halo of the temperature modulation around the heat sources. From the amplitude image (a) it is hardly possible to judge which of the bright regions are real heat sources and which are regions of high emissivity. In the phase image (b) and the 0°/-90° image (c), however, this emissivity contrast is indeed perfectly removed. Only the signal-to-noise ratio is degraded in regions of a low emissivity. The differences between the phase image (b) and the 0°/-90° one (c) are clearly visible in Fig. 3. The phase image (b) shows a stronger halo around the heat sources, and it displays heat sources of different intensity in a comparable brightness ("dynamic compression" feature). On the other hand, the 0°/-90° image (c) shows a lower blurring and displays heat sources of different power with different brightness. The power distribution (d) which was deconvoluted from (c) reveals many more details than the original images.

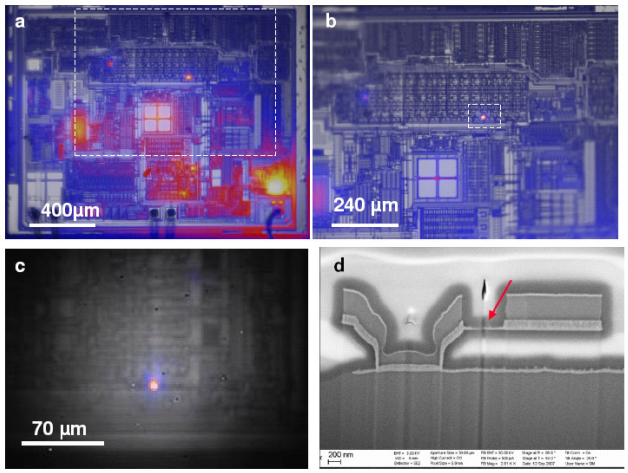

Fig. 4: (a) Survey image of the whole die (objective 2.5×), (b) detail image of the region framed in (a) (objective 5×), (c) Detail image of the region framed in (b) (objective 5× with SIL), (d) SEM image of a cross section through the fault region

In the next example overlay images of the topography image (in grey) with the actual LIT images (in color) of a faulty device are shown. Fig. 4 (a) was taken at a lock-in frequency of 10 Hz by using a 2.5× objective which is able to display the whole die. By comparing the heat transportation of the defective device to a reference, the point-like power source in the framed region could be identified as defect-

related thermal emission. In order to allow a better localization of the thermal emission to the single device components (b), a 5× objective was used and the lock-in frequency was increased to 25 Hz. Finally, (c) shows the region around the fault imaged at the same frequency through a silicon solid immersion lens (SIL), which further increased the magnification by a factor of 3.5. The localization of the fault allowed a focused ion beam (FIB) preparation of a cross-section specimen for a scanning electron microscopy (SEM) investigation, which is shown in (d). This image shows residues of a TiN barrier layer which were not completely etched away (arrow) and finally lead to a short. This case study shows the usefulness of LIT at IC investigations due to the fact that even defects which are orders of magnitude smaller than the resulting spatial resolution are detectable.

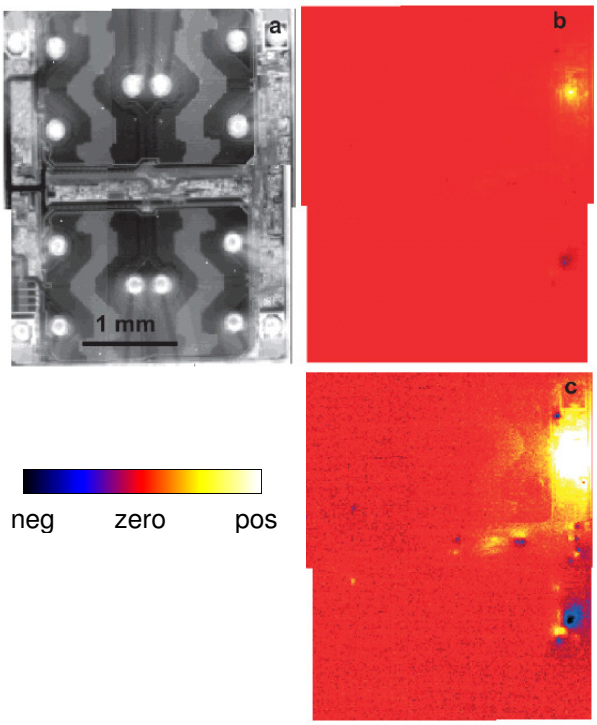

Fig. 5: Topography image (a) and fixed phase lock-in thermogram: (b) and (c) of an IC with permanently applied supply voltage and triggered control input. (c) is a contrast-enhanced presentation of (b)

In the next example in Fig. 5, which was an intact step motor controller, the supply voltage was permanently applied and the lock-in trigger was fed to a control input. In this arrangement permanently existing heat sources in the device, which are not affected by the trigger signal, do not appear in the lock-in thermogram. Only heat sources affected by the trigger signal are detected here. In a single phase image (approx. -45°) it can be distinguished whether heat is generated in the on-state or in the off-state of the trigger (positive or negative response). In Fig. 5 (b) and (c) complementary acting heat sources are made visible by bright and dark spots. In a similar way certain activities in a logic device can be switched on or off, synchronized to the lock-in correlation, which would allow an easy functional in-circuit test of complex logical devices based on lock-in thermography.

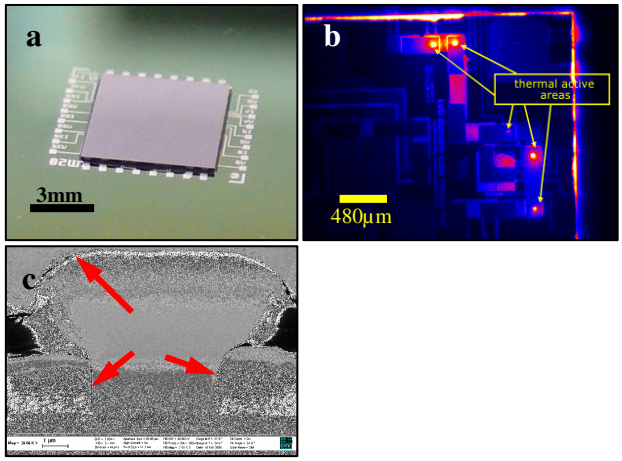

Fig. 6: Picture of the flip chip device (a), LIT result shows thermally active areas (b), SEM investigations of a contact cross section reveals additional insulator layer (red arrows in c)

In addition, Lock-in Thermography is also applicable for backside inspection. Figure 6 shows the investigation of a flip chip device with local high ohmic contacts. Due to the fact that silicon is IR transparent (dependent on its doping concentration) it is possible to

investigate the inner structure non-destructively. A mechanical cross section and SEM investigations were able to determine the root cause – an additional insulator layer infiltration in the contact area [12].

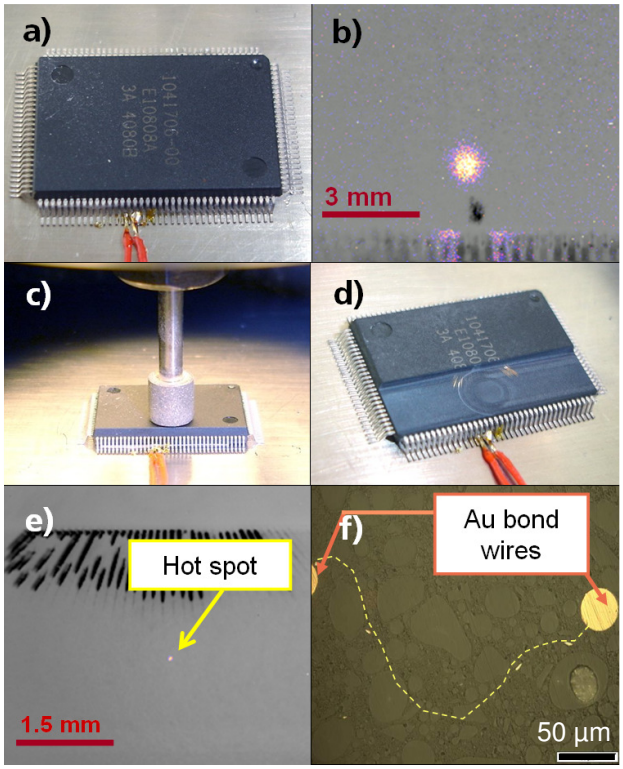

Fig. 7: Picture of the fully packaged device (a) and first LIT measurements (b), mechanical grinding of package material (c, d) allow defect allocation between bond wires (e), cross section show path of a metal splinter creating a short (f, light microscope image)

Besides the advantages of using Lock-in Thermography in case of single chip devices especially the opportunity of investigating fully packaged devices is an important advantage in comparison to other failure detection methods. Note that thermal waves penetrate even optically opaque materials like mould compounds. Due to the damping of thermal waves, using a lock-in frequency of 1 to 25 Hz allows the observation of hot spots through 100-400 µm package material with a lateral spot size of only a few tens to hundred µm. Even if the spatial resolution is not good enough to allow the detection of a single defect electrical component, this is extremely helpful especially in case of defective bond areas or stacked die devices. It gives the opportunity of deciding the next preparation steps and, most important, preserves the overall electrical functionality of the device. Such investigations cannot be done by optical methods like OBIRCH or light emission microscopy. Figure 7 gives an example for the usefulness of this allocation method where a hot spot due to a metal splinter occurred in the bonding area. After first hot spot allocation (b), the package material was grinded mechanically and a second LIT measurement (e) allocated the root cause between to bond wires which was proven by a mechanical cross section.

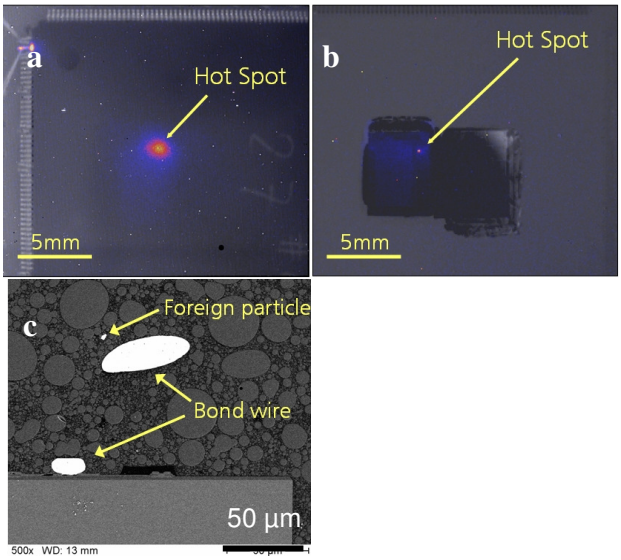

Fig. 8: LIT result at a fully packaged stacked die device (a) and after opening using chemical etching (b), SEM investigations of the cross section show foreign Al particle (c)

In case of the investigations at a stacked die device given in Fig. 8 LIT results reveal a hot spot not in the bond but in the chip area. Therefore, an opening using chemical etching was possible allowing a better spatial

resolution. Again, cross sectioning and SEM/ EDX investigations were applied determining an Al-splinter as root cause. Furthermore, a 3D defect localization at fully packaged multi chip modules by analyzing the phase quantitatively is part of research, these days.

Summary and outlook

Lock-in IR thermography, which was already established as a standard technique in non-destructive testing and solar cell research, has now successfully entered the field of IC failure analysis. In comparison with other thermal failure analysis techniques (liquid crystal microscopy, fluorescence microthermal imaging; also stabilized, stabilized moiré imaging, Schlieren imaging, Raman IR thermography, conventional IR microscopy) it shows the following advantages:

1. The thermal sensitivity may be below 100 µK (depending on the measurement time and the NA of the IR lens), which is 2-3 orders of magnitude better than that of previous techniques. Thus, LIT can be applied to investigate also weak heat sources, which have been non-accessible by thermal methods previously.

2. It requires no foreign layer at the surface, hence it also is used on a wafer scale.

3. The measurement procedure and the interpretation of the results are very straightforward: One needs no temperature stabilization and no shading of the setup, there is no degradation, and heat sources appear simply as bright spots in the images.

4. It also is used as a backside analysis technique. In case of highly doped bulk silicon LIT can also be applied, similar to investigations through opaque materials like mould compound.

5. Due to the dynamic nature of the measurement, lateral heat conduction is considerably reduced. Hence, the effective spatial resolution is improved compared to steady-state thermal imaging techniques.

6. Non-destructive defect localization at fully packaged devices is possible, though with degraded spatial resolution, which preserves the overall functionality and allows a better evaluation of the following preparation steps and failure analysis methods.

One of the general problems of conventional IR microscopy, the emissivity contrast artefact, can be overcome in 2-phase Lock-in Thermography by displaying the phase image or the 0°/-90° image, which are both inherently emissivity-corrected. The spatial resolution, which is diffraction-limited for mid-range IR cameras to about 3.6 µm, can be improved to nearly 1 µm by applying a solid immersion lens.

Acknowledgements

The authors like to thank Achim Lindner (Micronas GmbH), Jürgen Schulz (Melexis GmbH) and Volkmar Gottschalk (ELMOS Semiconductors) for providing samples and J.-M. Wagner for critically reading the manuscript. The work was supported by the European project Pidea “Full control”.

References

1. P.K. Kuo, T. Ahmed, H. Jin, and R.L. Thomas, *Phase-Locked Image Acquisition in Thermography, SPIE* **1004**, 41-45 (1988)

2. X.P.V. Maldague, *Theory and Practice of Infrared Technology for Nondestructive Testing,* Wiley, New York (2001)

3. O. Breitenstein and M. Langenkamp, *Lock-in Thermography – Basics and Use for Functional Diagnostics of Electronic Components,* Springer, Berlin, Heidelberg (2003), new edition in 2010

4. O. Breitenstein, J.P. Rakotoniaina, F. Altmann, J. Schulz, and G. Linse, *Fault Localization and Functional Testing of ICs by Lock-in Thermography, Proc. 28th ISTFA,* 29-36 (2002)

5. O. Breitenstein, J.P. Rakotoniaina, F. Altmann, T. Riediger, M. Gradhand, *New Developments in IR Lock-in Thermography, Proc. 30th ISTFA,* 595-599 (2004)
6. M. Gradhand, O. Breitenstein, *Preparation of non conducting infrared-absorbing thin films*, Review of Scientific Instruments **76**, 053702 (2005)
7. F. Altmann, T. Riediger, O. Breitenstein, *Fault Localization of ICs by Lock-in Fluorescent Microthermal Imaging (Lock-in FMI)*, Poster at *30th ISTFA (2004)*; see also O. Breitenstein et al., *Lock-in Thermography – A New FA Tool*, tutorial at *ISTFA 2005*
8. J.B. Colvin, *Moiré Stabilized Thermal Imaging*, *Proc. 12th IPFA* (2005), 163-166
9. E. Hecht: *Optics*. Addison-Wesley, San Francisco, CA (2002)
10. O. Breitenstein, F. Altmann, T. Riediger, D. Karg, V. Gottschalk, *Use of a Solid Immersion Lens for Thermal IR Imaging, Proc. 32nd ISTFA*, 382-388 (2006)
11. H. Suzuki, K. Koshikawa, T. Kuroda, T. Ishizuka, F.P. Gyue, F.P. Yuan, W.J. Ji, *Improvement of Performance for Higher Magnification Thermal Imaging*, *Proc. 16th IPFA 2009,* 489 - 492 (2009)
12. C. Schmidt, M. Simon, F. Altmann, *Failure analysis of stacked-die devices by combining non-destructive localization and target preparation methods, Proc. 35nd ISTFA*, 319-323 (2009)